

②

ARL-FLIGHT-MECH-R-180

AR-005-600



**DTIC** FILE COPY

**DEPARTMENT OF DEFENCE**

**DEFENCE SCIENCE AND TECHNOLOGY ORGANISATION**

**AERONAUTICAL RESEARCH LABORATORY**

**MELBOURNE, VICTORIA**

**AD-A228 450**

Flight Mechanics Report 180

**A FLIGHT DYNAMIC MODEL OF AIRCRAFT SPINNING**

by

S.D. Hill and C.A. Martin

**DTIC**  
**ELECTE**  
**NOV 13 1990**  
**S E D**

Approved for public release.

(C) COMMONWEALTH OF AUSTRALIA 1990

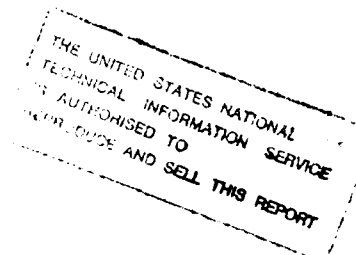
JUNE 1990

This work is copyright. Apart from any fair dealing for the purpose of study, research, criticism or review, as permitted under the Copyright Act, no part may be reproduced by any process without written permission. Copyright is the responsibility of the Director Publishing and Marketing, AGPS. Inquiries should be directed to the Manager, AGPS Press, Australian Government Publishing Service, GPO Box 84, CANBERRA ACT 2601.

AR-005-600

**DEPARTMENT OF DEFENCE  
DEFENCE SCIENCE AND TECHNOLOGY ORGANISATION  
AERONAUTICAL RESEARCH LABORATORY**

Flight Mechanics Report 180



**A FLIGHT DYNAMIC MODEL OF AIRCRAFT SPINNING**

by

S.D. Hill and C.A. Martin

**SUMMARY**

*A flight dynamic model of aircraft spinning has been developed. It is capable of simulating aircraft behaviour from conventional flight through stall, spin entry, steady spin, and spin recovery. A data base storage technique has been used to provide the six force and moment coefficients required. The data base embodies rotary balance data measured for a basic training aircraft plus computed small disturbance data calculated from a line vortex model.*



**(C) COMMONWEALTH OF AUSTRALIA 1990**

---

**POSTAL ADDRESS:** Director, Aeronautical Research Laboratory,  
P.O. Box 4331, Melbourne, Victoria, 3001, Australia

## Contents

<b>NOTATION</b>	<b>3</b>
<b>1 INTRODUCTION</b>	<b>5</b>
<b>2 FLIGHT DYNAMIC SPIN MODEL</b>	<b>5</b>
<b>3 SPIN MODEL DATA BASE DETAILS</b>	<b>6</b>
3.1 Methods of Aircraft Simulation . . . . .	6
3.2 Source of Rotary Balance Data Base . . . . .	7
3.3 Limits on Available Data . . . . .	7
3.3.1 Decoupling of Aileron Data . . . . .	8
3.3.2 Generating Positive Sideslip Angle Data . . . . .	9
3.3.3 Data Base Processing . . . . .	11
<b>4 TRIM ROUTINES</b>	<b>11</b>
4.1 Steady Spin Trimming . . . . .	12
4.2 Steady Rectilinear Flight Trimming . . . . .	14
<b>5 DECOMPOSITION OF AIRCRAFT ANGULAR MOTION</b>	<b>15</b>
5.1 Small Disturbance Data . . . . .	17
<b>6 EXAMPLE APPLICATION OF THE SPIN MODEL</b>	<b>18</b>
6.1 Equilibrium Spin Prediction . . . . .	18
6.2 Spin Manoeuvre . . . . .	18
<b>7 CONCLUSION</b>	<b>20</b>
<b>REFERENCES</b>	<b>21</b>
<b>FIGURES</b>	<b>22</b>
<b>DISTRIBUTION</b>	<b>22</b>
<b>DOCUMENT CONTROL DATA</b>	<b>22</b>



1

Accession For	
NTIS GRA&I	<input checked="" type="checkbox"/>
DTIC TAB	<input type="checkbox"/>
Unannounced	<input type="checkbox"/>
Justification	
By	
Distribution/	
Availability Codes	
Dist	Avail and/or Special
A-1	

## NOTATION

alt	Altitude
$b$	Wing span
$\bar{c}$	Mean aerodynamic chord
$C_D$	Drag force coefficient = $\frac{\text{Drag force}}{\frac{1}{2}\rho V^2 S}$
$CG$	Centre of gravity
$C_L$	Lift force coefficient = $\frac{\text{Lift force}}{\frac{1}{2}\rho V^2 S}$
$C_R$	Total force coefficient = $\sqrt{C_L^2 + C_D^2}$
$C_X$	Axial force coefficient = $\frac{\text{Axial force}}{\frac{1}{2}\rho V^2 S}$
$C_Y$	Side force coefficient = $\frac{\text{Side force}}{\frac{1}{2}\rho V^2 S}$
$C_Z$	Normal force coefficient = $\frac{\text{Normal force}}{\frac{1}{2}\rho V^2 S}$
$C_l$	Rolling moment coefficient = $\frac{\text{Rolling moment about centre of gravity}}{\frac{1}{2}\rho V^2 S b}$
$C_{l_p}, C_{l_q}, C_{l_r}$	Rolling moment coefficient w.r.t. roll, pitch, and yaw rates respectively
$C_m$	Pitching moment coefficient = $\frac{\text{Pitching moment about centre of gravity}}{\frac{1}{2}\rho V^2 S c}$
$C_{m_p}, C_{m_q}, C_{m_r}$	Pitching moment coefficient w.r.t. roll, pitch, and yaw rates respectively
$C_n$	Yawing moment coefficient = $\frac{\text{Yawing moment about centre of gravity}}{\frac{1}{2}\rho V^2 S b}$
$C_{n_p}, C_{n_q}, C_{n_r}$	Yawing moment coefficient w.r.t. roll, pitch, and yaw rates respectively
$g$	Gravitational constant
$I_X, I_Y, I_Z$	Moments and product of inertia
$L_{Bw}$	Vector transformation matrix from wind axes to body axes
$m$	Aircraft mass
$p$	Roll rate about body axes
$q$	Pitch rate about body axes
$R_s$	Spin radius measured from the spin axis to the aircraft's CG
$r$	Yaw rate about body axes
$S$	Aircraft wing area
$V$	Flight path velocity

$\alpha$	Angle of attack
$\beta$	Sideslip angle
$\delta_a$	Aileron deflection, positive when right aileron is down, (stick left)
$\delta_e$	Elevator deflection, positive when trailing edge is down, (stick forward)
$\delta_r$	Rudder deflection, positive when trailing edge is port, (port pedal forward)
$\theta$	Euler pitch angle
$\rho$	Freestream density
$r_0, r_1, r_2, r_3$	Aircraft attitude quaternions
$\sigma$	Helix angle = $\tan^{-1} \frac{R_S \Omega}{V}$
$\phi$	Euler roll angle
$\psi$	Euler yaw angle
$\Omega$	Spin rate along flight-path
$\frac{\Omega}{2V}$	Spin coefficient, same sense as $\Omega$

### Superscripts

- Rate of change of, (derivative of)

### Subscripts

- B Body axes
- r Rotary balance
- S Stability axes
- o Small disturbance
- W Wind axes

## 1 INTRODUCTION

This report documents the development of a flight dynamic model of aircraft spinning which has been written using the Advanced Continuous Simulation Language (ACSL). The flight dynamic model has the facility to simulate time history manoeuvres from both rectilinear flight and from steady spin conditions and provides information on the aerodynamic forces and aircraft motion. The model is applied to a basic training aircraft design which is intended to have good characteristics for demonstrating spin entry, steady spins, and spin recovery.

The aerodynamic data required by the flight dynamic model has been stored in data base format and consists of wind tunnel rotary balance data from a basic training aircraft and computed disturbance data. The problems with producing such a data base to cover a large flight regime are discussed in Section 3. The flight dynamic trimming methods are described in Section 4, and Section 5 presents the development of angular rate equations needed to calculate the disturbance moment contributions.

Two example applications of the flight dynamic model are presented in Section 6 to illustrate the capabilities of the model. One gives an example of equilibrium spin prediction; the other demonstrates a spin entry and recovery manoeuvre for which various methods of presentation of the output time history data have been supplied.

## 2 FLIGHT DYNAMIC SPIN MODEL

The six degree of freedom air-path (SDOFAP) aircraft simulation program SDOFAP of Reference 1 has been used as the framework for the flight dynamic spin model program (FDSM). This program is written in the Advanced Continuous Simulation Language (ACSL) (Reference 2) and can be supplemented with user-supplied FORTRAN subroutines. The SDOFAP model provides a comprehensive means by which to represent the aircraft's characteristics by supplying user-defined subroutines for the X,Y,Z,L,M,N aerodynamic and propulsive forces and moments. For the flight dynamic spin model the aerodynamic forces and moments are derived from wind-tunnel rotary-balance data in conjunction with computed disturbance moment data.

In order to eliminate the problems of singularities using Euler angle rate equations, the simulation program employs quaternions to represent the aircrafts attitude. Quaternion time derivatives are always finite and continuous and only require four integrations with one constraint equation, whereas the direction cosines generated from the Euler angles require nine integrations and six constraint equations.

The state variables for the flight dynamic model that are integrated over the

time history are:

$$\begin{array}{lcl}
 \alpha & \left. \begin{array}{l} \alpha \\ \beta \\ V \end{array} \right\} & \text{flight path variables} \\
 \beta & & \\
 V & & \\
 p & \left. \begin{array}{l} p \\ q \\ r \end{array} \right\} & \text{body rotation rates} \\
 q & & \\
 r & & \\
 r_0 & \left. \begin{array}{l} r_0 \\ r_1 \\ r_2 \\ r_3 \end{array} \right\} & \text{attitude quaternions} \left\{ \begin{array}{l} \psi \text{ Euler} \\ \theta \text{ angles} \\ \phi \end{array} \right. \\
 r_1 & & \\
 r_2 & & \\
 r_3 & & \\
 x & \left. \begin{array}{l} x \\ y \\ \text{alt} \end{array} \right\} & \text{displacements} \\
 y & & \\
 \text{alt} & &
 \end{array}$$

The aerodynamic force and moment contributions for the Wamira spin model data comprise the following rotary balance and disturbance terms:

$$\begin{aligned}
 X &= X_r \\
 Y &= Y_r \\
 Z &= Z_r \\
 L &= L_r + L_o \\
 M &= M_r + M_o \\
 N &= N_r + N_o
 \end{aligned}$$

The decomposition of the aircraft motion into steady rotating and disturbance components is described in Section 5. The control inputs used to manoeuvre the aircraft are:

$$\begin{aligned}
 \delta_e \\
 \delta_r \\
 \delta_a
 \end{aligned}$$

### 3 SPIN MODEL DATA BASE DETAILS

#### 3.1 Methods of Aircraft Simulation

An important consideration in constructing a flight dynamic model is the representation of the aerodynamic forces and moments. Reference 3 provides a summary of dynamic modelling procedures under consideration for high rotation rate non-linear manoeuvres. These are listed below:

1. Polynomial Model: A Taylor expansion of the force functions about an equilibrium condition yielding aerodynamic forces in derivative form.
2. Tobak and Schiff Formulation: A comprehensive development of mathematical models which can represent all types of non-linear time dependent motion.
3. Data Table Representation: Aerodynamic data stored in table form. This enables the forces to be represented as arbitrary non-linear functions of a number of independent variables.
4. Rotary Balance Data: Rotary balances enable the model to be rotated at constant incidence angles to the velocity vector, and over a range of rotation rates creating an extensive non-linear steady rotation data base of information.

Of these four methods the Rotary Balance (RB) method was implemented, using an extensive RB data base collected on a  $\frac{1}{4}$ th scale model of the Wamira. This experimental data is augmented by computed aerodynamic moment data required to describe the additional forces occurring during the non-steady parts of the manoeuvres.

### 3.2 Source of Rotary Balance Data Base

A Wamira spin-model RB data base has been developed from RB spin-model measurements carried out at the NASA Langley Research Centre (LRC), in June 1983 by Bihrie Applied Research Inc. (BAR). The results of this testing have been reported in References 4 and 5 and subsequently presented in graphical form in Reference 6.

Simulating an aircraft's dynamic behaviour using an aerodynamic data base requires that data be generated to cover the full range of state and control variables involved. The data produced at NASA LRC covered a wide range of angle of attack ( $\alpha$ ), sideslip angle ( $\beta$ ), and spin rate ( $\Omega$ ) conditions, combined with variations in elevator ( $\delta_e$ ), rudder ( $\delta_r$ ), and aileron ( $\delta_a$ ) deflection. For a given control deflection, the  $\alpha$  range was  $0^\circ$  to  $90^\circ$ , the  $\beta$  range was  $-10^\circ$  to  $0^\circ$ , and the non-dimensional spin rate ( $\frac{\Omega b}{V}$ ) range was  $-0.6$  to  $0.6$ . The settings of control deflection tested were  $\delta_e : -25^\circ, 0^\circ, 23^\circ$ ;  $\delta_r = -25^\circ, 0^\circ, 25^\circ$ ;  $\delta_a = -18^\circ, 0^\circ, 18^\circ$ . However not all possible control deflection combinations were tested.

### 3.3 Limits on Available Data

The flight dynamic spin model requires the aerodynamic forces and moments  $X, Y, Z, L, M, N$  to be calculated, therefore the RB data needed are  $C_X, C_Y, C_Z$  (axial, side, normal-force non-dimensional coefficients respectively), and  $C_l, C_m, C_n$  (roll, pitch, yaw-moment coefficients respectively). Assuming that all the control inputs

are coupled, (ie. a change in rudder deflection will affect the influence of the elevator etc.), then the six force and moment coefficients will be coupled functions of the three control inputs and the three state variables as follows:

$$C_X = f_n\{\delta_e, \delta_r, \delta_a, \beta, \alpha, \frac{\Omega}{2V}\} \quad (1)$$

and similarly for  $C_Y, C_Z, C_l, C_m, C_n$ . The generation of a data base needed to describe the non-linear variation of the six aerodynamic coefficients with the three control settings and the three flow-angle states allowing for full coupling would require a prohibitively large test program. For the Wamira, measurements were made at ten angles-of-attack, eleven rotation rates, and two sideslip angles for a large combination of control deflections with zero and maximum setting angles. This means that data is required for at least 27 control deflection states (ie. combinations of  $\delta_e$  : -ve, zero, +ve  $\delta_r$  : -ve, zero, +ve  $\delta_a$  : -ve, zero, +ve) to provide an efficient interpolation scheme as shown in Figure 1. However the data available does not cover the full range of aileron deflections required to set up such a scheme.

### 3.3.1 Decoupling of Aileron Data

Since only a small number of aileron control configurations were tested in Reference 4, the possibility of decoupling the effect of the aileron from both the elevator and rudder was investigated. By examining tests carried out on model configurations with constant rudder and elevator, but with variations of aileron ( $\delta_a$  :  $-18^\circ, 0^\circ, 18^\circ$ ), the degree of coupling can be found. The tests available were:

1.  $\delta_e = -25^\circ, \delta_r = 0^\circ, \delta_a = 0^\circ$
2.  $\delta_e = -25^\circ, \delta_r = 0^\circ, \delta_a = 18^\circ$
  
3.  $\delta_e = -25^\circ, \delta_r = -25^\circ, \delta_a = -18^\circ$
4.  $\delta_e = -25^\circ, \delta_r = -25^\circ, \delta_a = 0^\circ$
5.  $\delta_e = -25^\circ, \delta_r = -25^\circ, \delta_a = 18^\circ$
  
6.  $\delta_e = 0^\circ, \delta_r = -25^\circ, \delta_a = 0^\circ$
7.  $\delta_e = 0^\circ, \delta_r = -25^\circ, \delta_a = 18^\circ$
  
8.  $\delta_e = 0^\circ, \delta_r = 25^\circ, \delta_a = -18^\circ$
9.  $\delta_e = 0^\circ, \delta_r = 25^\circ, \delta_a = 0^\circ$

Calculating the difference between these four groups of test data gives two incremental blocks of data ( $C_X, C_Y, C_Z, C_l, C_m, C_n$ ) for  $\delta_a = -18^\circ$  (ie. configurations 3 - 4; 8 - 9), and three incremental blocks for  $\delta_a = 18^\circ$  (configurations 2 - 1; 5 - 4; 7 - 6). The result of this differencing shows that  $\Delta C_X, \Delta C_Y, \Delta C_l$  and  $\Delta C_n$  are close to zero and therefore can be considered independent of elevator and rudder control.  $\Delta C_Z$  and  $\Delta C_m$  however, do show evidence of coupling but when

compared to the overall magnitude of  $C_Z$  and  $C_m$ , the  $\delta_a$  increments are of less significance than the influence of  $\delta_e$  and  $\delta_r$ . This is convenient because now the aileron contribution for the forces and moments can be simply added as an increment to the elevator and rudder data blocks as follows:

$$C_X = C_X\{\delta_e, \delta_r, \beta, \alpha, \frac{\Omega b}{2V}\} + dC_X\{\delta_a, \beta, \alpha, \frac{\Omega b}{2V}\} \quad (2)$$

Note that this implies that when  $\delta_a = 0$ ,  $dC_X = 0$ , etc.

Since only one incremental data block is needed for each aileron control setting the two  $\delta_a = -18^\circ$  data blocks have been averaged. Similarly the three  $\delta_a = 18^\circ$  data blocks have been averaged. Obviously for  $\delta_a = 0^\circ$  all incremental data is zero and no data block is needed. This new data base scheme is shown in Figure 2.

The creation of the incremental aileron data blocks also solved another problem caused by limited control deflection data. The following control deflections were not covered in the NASA LRC test sequence:

1.  $\delta_e = 23^\circ$ ,  $\delta_r = -25^\circ$ ,  $\delta_a = 0^\circ$
2.  $\delta_e = -25^\circ$ ,  $\delta_r = 25^\circ$ ,  $\delta_a = 0^\circ$

However, the following control deflections with aileron were available:

3.  $\delta_e = 23^\circ$ ,  $\delta_r = -25^\circ$ ,  $\delta_a = 18^\circ$
4.  $\delta_e = -25^\circ$ ,  $\delta_r = 25^\circ$ ,  $\delta_a = -18^\circ$

By subtracting the incremental aileron data blocks formed above from the  $18^\circ$  and  $-18^\circ$  aileron configuration, (3. and 4. above.), data for zero aileron cases, (1. and 2. above.), can be created.

### 3.3.2 Generating Positive Sideslip Angle Data

The only configuration tested at NASA LRC for both positive and negative  $\beta$  angles was for  $\delta_e = \delta_r = \delta_a = 0^\circ$ , where the  $\beta$  settings were  $-10^\circ, 0^\circ, 10^\circ$ . All other configurations were tested for  $\beta = -10^\circ$  and  $0^\circ$  since preliminary calculations showed that equilibrium sideslip angle for positive spin rates could be expected to lie within this range. For the general unsteady manoeuvres occurring during spin entry and recovery both positive and negative sideslip angles can be expected to occur. However the  $\beta = 10^\circ$  data can be generated by assuming that the aerodynamic changes due to  $\beta$ ,  $\Omega$ , and  $\delta_r$  are symmetrical, although in practice it is difficult to achieve symmetrical conditions in a wind-tunnel environment. Take for example an aircraft

spinning with the following conditions:

$$\begin{aligned}\delta_e &= 25^\circ \\ \delta_r &= -25^\circ \\ \delta_a &= 0^\circ \\ \beta &= -10^\circ \\ \alpha &= 60^\circ \\ \frac{\Omega b}{2V} &= -0.6\end{aligned}$$

To make the spin rate opposite to the current spin rate, (ie. port spin to starboard spin), the conditions would have to be as follows:

$$\begin{aligned}\delta_e &= 25^\circ \\ \delta_r &= 25^\circ \\ \delta_a &= 0^\circ \\ \beta &= 10^\circ \\ \alpha &= 60^\circ \\ \frac{\Omega b}{2V} &= 0.6\end{aligned}$$

Note that  $\delta_r, \beta$ , and  $\frac{\Omega b}{2V}$  only have changed sign. This means that data points at negative  $\beta$  can be used for positive  $\beta$  with opposite spin through the assumption of spin symmetry. Below is an example of how the positive  $\beta$  data is calculated. Figures 3 and 4 show this graphically.

$$C_l\{\delta_e = 25^\circ, \delta_r = -25^\circ, \beta = 10^\circ\} = -C_l\{\delta_e = 25^\circ, \delta_r = 25^\circ, \beta = -10^\circ\} \quad (3)$$

$$\begin{array}{lll} \frac{\Omega b}{2V} = -0.6 \rightarrow 0.6 & & \frac{\Omega b}{2V} = 0.6 \rightarrow -0.6 \\ \alpha = 0^\circ \rightarrow 90^\circ & & \alpha = 0^\circ \rightarrow 90^\circ \end{array}$$

and similarly for  $C_Y, C_n$ .

$$C_m\{\delta_e = 25^\circ, \delta_r = -25^\circ, \beta = 10^\circ\} = C_m\{\delta_e = 25^\circ, \delta_r = 25^\circ, \beta = -10^\circ\} \quad (4)$$

$$\begin{array}{lll} \frac{\Omega b}{2V} = -0.6 \rightarrow 0.6 & & \frac{\Omega b}{2V} = 0.6 \rightarrow -0.6 \\ \alpha = 0^\circ \rightarrow 90^\circ & & \alpha = 0^\circ \rightarrow 90^\circ \end{array}$$

and similarly for  $C_X, C_Z$ .

The same procedure could also be applied to the aileron incremental block data, but this was not required. The aileron data only shows minimal change due to  $\beta$  and has therefore been taken to be independent of  $\beta$ . All aileron incremental data blocks are those for  $\beta = 0^\circ$  and are constructed as follows:

$$dC_X = f_n\{\delta_a, \alpha, \frac{\Omega b}{2V}\} \quad (5)$$

and similarly for  $dC_Y, dC_Z, dC_l, dC_m, dC_n$ . The total collated data for the model then becomes:

$$\begin{aligned} C_X &= C_X\{\delta_e, \delta_r, \beta, \alpha, \frac{\Omega b}{2V}\} + dC_X\{\delta_a, \alpha, \frac{\Omega b}{2V}\} \\ C_Y &= C_Y\{\delta_e, \delta_r, \beta, \alpha, \frac{\Omega b}{2V}\} + dC_Y\{\delta_a, \alpha, \frac{\Omega b}{2V}\} \\ C_Z &= C_Z\{\delta_e, \delta_r, \beta, \alpha, \frac{\Omega b}{2V}\} + dC_Z\{\delta_a, \alpha, \frac{\Omega b}{2V}\} \\ C_l &= C_l\{\delta_e, \delta_r, \beta, \alpha, \frac{\Omega b}{2V}\} + dC_l\{\delta_a, \alpha, \frac{\Omega b}{2V}\} \\ C_m &= C_m\{\delta_e, \delta_r, \beta, \alpha, \frac{\Omega b}{2V}\} + dC_m\{\delta_a, \alpha, \frac{\Omega b}{2V}\} \\ C_n &= C_n\{\delta_e, \delta_r, \beta, \alpha, \frac{\Omega b}{2V}\} + dC_n\{\delta_a, \alpha, \frac{\Omega b}{2V}\} \end{aligned} \quad (6)$$

This is depicted in Figure 5. The next stage is to determine a means by which to access this data efficiently.

### 3.3.3 Data Base Processing

A data base processing program library has been developed to read, store, and interpolate/extrapolate the Wamira spin data as represented in the data base schematic of Figure 5. Basically each force and moment, (or arbitrary data), has been defined as a variable function with a set of input variables. In FORTRAN the axial force coefficient would be accessed as follows:

$$CX = CX\_DATA(DELE, DELR, BETA, ALPHA, OMEGA) + DCX(DELA, ALPHA, OMEGA)$$

where DELE, DELR, DELA, BETA, ALPHA, OMEGA can be any arbitrary value. All interpolation/extrapolation is calculated within the function CX\_DATA and therefore does not interfere with the flow of the equations of motion for the aerodynamic routines.

## 4 TRIM ROUTINES

It is preferable to begin simulation with all the equations of motion in trim. This means that all accelerations must be zero along and about the body axes of the aircraft. The Wamira flight dynamic model has been developed to trim in either

steady spin or steady rectilinear flight through the use of two trimming routines. Each of the two trim conditions is calculated in two trim phases; the first phase provides an approximate initial trim, and the second uses these values in a more intensive search routine to provide more accurate trim conditions using the flight dynamic equations within the ACSL program.

#### 4.1 Steady Spin Trimming

The initial approximate spin trimming is achieved using approximate equilibrium spin equations and follows the approach presented in Reference 7. Following the assumptions given in Reference 7, Figure 6 shows the orientation of the forces and axes of an aircraft in a steady spin. The equations given below show the balance of forces in a steady spin:

$$mg = \frac{1}{2}\rho V^2 SC_D \quad (7)$$

$$mR_S\Omega^2 = \frac{1}{2}\rho V^2 SC_L \quad (8)$$

Note that in this approximation the side forces are assumed to be zero. The aerodynamic moments of Equation (6) are balanced by the following inertial moments:

$$C_m = (4/\rho S \bar{c} b^2)(\frac{\Omega b}{2V})^2(I_X - I_Z) \sin 2\alpha \cos^2(\sigma + \beta) \quad (9)$$

$$C_l = (4/\rho S b^3)(\frac{\Omega b}{2V})^2(I_Z - I_Y) \sin \alpha \sin 2(\sigma + \beta) \quad (10)$$

$$C_n = (4/\rho S b^3)(\frac{\Omega b}{2V})^2(I_Y - I_X) \cos \alpha \sin 2(\sigma + \beta) \quad (11)$$

where

$$\begin{aligned} \sigma &= \tan^{-1} \frac{R_S \Omega}{V} \\ &= \tan^{-1} \left\{ \frac{\rho S b C_L}{4m(\frac{\Omega b}{2V})} \right\} \end{aligned} \quad (12)$$

These equations must be solved simultaneously to trim for a steady spin. A numerical solution which exploits the nature of the forces and gives added physical insight can be achieved by sequentially processing the pitching, rolling, and yawing moment equations (Equations (9),(10),(11) respectively). For constant control deflections the inertia terms on the right hand side of the equations are a function of  $\alpha$ ,  $\frac{\Omega b}{2V}$ , and  $\beta$ . This is also true of the aerodynamic coefficients as indicated by Equation (6) of Section 3.3.2. The  $\alpha$ ,  $\frac{\Omega b}{2V}$  and  $\beta$  equilibrium values can be determined as follows.

The pitching moment equation is first solved for  $\frac{\Omega b}{2V}$  for the range of test  $\alpha$  values (here  $0 \rightarrow 90^\circ$ ) using Equation (9), with  $\beta$  taken as zero since  $C_m$  is not a strong function of  $\beta$  for most aircraft, aerodynamically and inertially. This produces a series of  $\alpha$  and  $\frac{\Omega b}{2V}$  values that satisfy the pitching moment equation as shown in Figure 7. These are then used in the rolling moment equation to solve for  $\beta$  (Equation (10)). The rolling moment equation is a strong function of  $\beta$  in both aerodynamic and inertial terms, and by solving for  $\beta$  with the previously formed series of  $\alpha$  and  $\frac{\Omega b}{2V}$ , a new series of data is formed that satisfies both the pitching and rolling moment equations as shown in Figure 8.

At this stage if required, a feed back loop can be implemented to update the  $\beta = 0$  condition used in the pitching moment equation (Equation (9)) to the new values just formed in Figure 8. However, this is only required if the aircraft configuration being studied shows signs of pitch sensitivity due to  $\beta$  using Equation (9). For the Wamira spin model data the correction is not significant and does not require the extra calculation.

Finally the yawing moment equation (Equation (11)) is used to find the combination of  $\alpha$ ,  $\frac{\Omega b}{2V}$ ,  $\beta$  of Figure 8 that satisfy all three moment equation. Each combination is substituted into both the aerodynamic and inertia terms of the yawing moment equation to find the intersection points as illustrated in Figure 9.

The intersection of the inertial and aerodynamic curves identifies the combination/s of  $\alpha$ ,  $\frac{\Omega b}{2V}$ ,  $\beta$  that satisfy all three moment equations for equilibrium in the spin. Only those intersections where the aerodynamic contribution has negative slope with respect to the inertia curve can result in a stable spin, (ie. stable equilibrium). Once  $\alpha$ ,  $\frac{\Omega b}{2V}$ , and  $\beta$  have been found for equilibrium, the drag and lift equations (Equations (7) and (8) respectively) can be used to find the descent velocity  $V$  and the spin radius  $R_s$ .

The initial body axis rotation rates can be calculated from Reference 7 using the helix angle from Equation (12) as follows:

$$p = \Omega \cos \alpha \cos(\beta + \sigma) \quad (13)$$

$$q = \Omega \sin(\beta + \sigma) \quad (14)$$

$$r = \Omega \sin \alpha \cos(\beta + \sigma) \quad (15)$$

and with the flight path angle  $\gamma$  approximately equal to  $90^\circ$ ,  $\theta$  and  $\phi$  are calculated as follows:

$$\theta \approx \alpha - \gamma \quad \{\gamma \approx 90^\circ\} \quad (16)$$

$$\phi \approx \beta + \sigma \quad (17)$$

This trim procedure is only the first part of the trim sequence. The flight dynamic spin model program uses these initial trim results to perform its own trimming of the six degree of freedom flight dynamic equations using the state variables defined in Section 2. This trim routine is called POWIT, (Reference 8), and is

a multivariable search technique for the solution of simultaneous non-linear equations. Basically POWIT, satisfies a given a set of condition constraints, by solving the full aerodynamic spin equations using a set of specified trimming variables that are incrementally changed. Solutions are found using a combination of search and gradient techniques, (detailed descriptions of these methods can be found in Reference 9). Upon exiting this routine the trimming variables define an accurate trim state. Figure 10 illustrates the procedure with a block diagram. For steady spin, the trimming variables and condition constraints are as follows:

<u>Trim variables</u>	<u>Condition constraints</u>
$\alpha$	$\dot{\alpha} = 0$
$\beta$	$\dot{\beta} = 0$
$V$	$\dot{V} = 0$
$\theta$	$\dot{\theta} = 0$
$\phi$	$\dot{\phi} = 0$
$p$	$\dot{p} = 0$
$q$	$\dot{q} = 0$
$r$	$\dot{r} = 0$
$\psi = 0$ fixed for given control setting angles.	$\dot{\psi} = \Omega$

#### 4.2 Steady Rectilinear Flight Trimming

For trimming in rectilinear flight the initial trim estimate is supplied by manual input. The initial estimate does not need to be accurate for rectilinear flight because with fewer variables, the trimming is more stable than for the spin. Steady rectilinear trimming is performed solely using POWIT and the following trimming variables and condition constraints are required to satisfy the flight dynamic equation block shown in Figure 10:

<u>Trim variables</u>	<u>Conditions constraints</u>
$\alpha$	$\dot{\alpha} = 0$
$\theta$	$\dot{V} = 0$
$\phi$	$\dot{\beta} = 0$
$\delta_e$	$\dot{q} = 0$
$\delta_r$	$\dot{r} = 0$
$\delta_a$	$\dot{p} = 0$
for given V and Thrust.	

Note, unlike the arrangement for trimming in the steady spin, the control deflections are not fixed but are used instead to trim the aircraft for a constant velocity

$V$  and powerplant thrust. Since the rotary balance measurements contain asymmetries in the lateral and directional forces for the steady symmetrical flight conditions, small control deflections  $\delta_a$ ,  $\delta_r$  are required for trim.

## 5 DECOMPOSITION OF AIRCRAFT ANGULAR MOTION

The basis of the proposed model formulation is the separation of the total angular motion into a component aligned with the flight path vector and a residual disturbance component. The aerodynamic forces and moments due to the former are identically those measured on a rotary balance, while the moments due to the residual disturbance are to be calculated from a simple aerodynamic model. The net forces at the c.g. due to the residual component have been taken to be zero in the present formulation. In other words, the residual component is modelled simply as a redistribution of the aerodynamic load without any change in the resultant X, Y, and Z components.

The method of separating the aligned component and the residual disturbance component was introduced by Reference 10. However, the equations derived assume the aircraft is descending vertically. The equations presented below do not make this assumption and therefore allow the prediction of aircraft behaviour during the transition from rectilinear flight to steady spin.

The rotation rate about the flight path vector can be calculated as follows (Reference 11 Equation (5.8,5)(c)).

$$p_w = p \cos \alpha \cos \beta + (q - \dot{\alpha}) \sin \beta + r \sin \alpha \cos \beta \quad (18)$$

Note,  $p_w$  is equal to the steady rotation rate ( $\Omega$ ) which is used for the rotary balance test. The  $\dot{\alpha}$  term in Equation (18) presents a problem because it is calculated using the forces read from the RB data base, but the forces can only be calculated after  $p_w$  is found. One solution is to iterate the system of equations until  $p_w$  and  $\dot{\alpha}$  converge on a steady value. Five iterations were found to be enough for an accurate convergence and once  $p_w$  ( $\Omega$ ) has been calculated, it is used to calculate the rotary and disturbance terms of  $p$ ,  $q$ ,  $r$  which are derived as follows.

From Equation (5.2,12) of Reference 11  $p$ ,  $q$ , and  $r$  may be calculated using  $p_w$ ,  $q_w$ , and  $r_w$  through rotations  $\alpha$  and  $\beta$ .

$$L_{WB} \begin{bmatrix} p \\ q \\ r \end{bmatrix} - \begin{bmatrix} p_w \\ q_w \\ r_w \end{bmatrix} = - \begin{bmatrix} 0 \\ 0 \\ 1 \end{bmatrix} \dot{\beta} + L_{WB} \begin{bmatrix} 0 \\ 1 \\ 0 \end{bmatrix} \dot{\alpha} \quad (19)$$

where  $L_{WB}$  is the matrix for transforming vectors from body axes to wind axes as follows:

$$L_{WB} = \begin{bmatrix} \cos \alpha \cos \beta & \sin \beta & \sin \alpha \cos \beta \\ -\cos \alpha \sin \beta & \cos \beta & -\sin \alpha \sin \beta \\ -\sin \alpha & 0 & \cos \alpha \end{bmatrix} \quad (20)$$

Now since

$$L_{BW} * L_{WB} = [I] \quad (21)$$

then

$$\begin{bmatrix} p \\ q \\ r \end{bmatrix} - L_{BW} \begin{bmatrix} p_W \\ q_W \\ r_W \end{bmatrix} = -L_{BW} \begin{bmatrix} 0 \\ 0 \\ 1 \end{bmatrix} \dot{\beta} + \begin{bmatrix} 0 \\ 1 \\ 0 \end{bmatrix} \dot{\alpha} \quad (22)$$

Equation (4.5,5) of Reference 11 gives:

$$L_{BW} = \begin{bmatrix} \cos \alpha \cos \beta & -\cos \alpha \sin \beta & -\sin \alpha \\ \sin \beta & \cos \beta & 0 \\ \sin \alpha \cos \beta & -\sin \alpha \sin \beta & \cos \alpha \end{bmatrix} \quad (23)$$

By substituting Equation (23) into Equation (22)  $p$ ,  $q$ , and  $r$  can be separated into components due to the rotation about the wind axes (ie. into its rotary part) and into the disturbance components as follows:

$$\begin{array}{lcl} p & = & p_W \cos \alpha \cos \beta \\ q & = & p_W \sin \beta \\ r & = & p_W \sin \alpha \cos \beta \end{array} \quad \left| \quad \begin{array}{l} -q_W \cos \alpha \sin \beta - r_W \sin \alpha + \dot{\beta} \sin \alpha \\ q_W \cos \beta + \dot{\alpha} \\ -q_W \sin \alpha \sin \beta + r_W \cos \alpha - \dot{\beta} \cos \alpha \end{array} \right. \quad (24)$$

rotary
disturbance

Now since the state equations of the flight dynamic model calculate  $p$ ,  $q$ , and  $r$  directly, the disturbance terms can be evaluated as follows to reduce the number of

mathematical calculations

$$\begin{aligned} p_o &= p - p_r \\ q_o &= q - q_r \\ r_o &= r - r_r \end{aligned} \quad (25)$$

Once the disturbance rotation rates are calculated using Equations (24) and (25) the disturbance moments can be found using the following equation and the calculated data base:

$$\begin{bmatrix} C_{l_o} \\ C_{m_o} \\ C_{n_o} \end{bmatrix} = \begin{bmatrix} C_{l_p} & C_{l_q} & C_{l_r} \\ C_{m_p} & C_{m_q} & C_{m_r} \\ C_{n_p} & C_{n_q} & C_{n_r} \end{bmatrix} \begin{bmatrix} p_o \\ q_o \\ r_o \end{bmatrix} \quad (26)$$

Only the diagonal terms of the moment coefficient matrix have so far been used to calculate the disturbance moments as these terms appear to be the most significant. The effect of the other terms has been assumed to be small and they are taken as zero. Future investigations into the disturbance coefficients will be undertaken to evaluate the influence of these smaller terms on predicted spin behaviour.

### 5.1 Small Disturbance Data

The rotary balance data was measured with the Wamira spin model performing steady rotations about an axis aligned with the freestream. This provides the steady aerodynamic moment data but does not supply the disturbance data that is required in this model formulation to represent the forces occurring in non-steady flight. The small disturbance coefficients included in Equation 26 represent the aerodynamic moments due to body rotation rates. The main diagonal terms, which have been included in the model, generally contribute damping forces in the aircraft response. A simple line vortex model has been developed to calculate these terms.

The line vortex model estimates the aerodynamic coefficients during steady rotation using line vortex representations of wing, tailplane, and fin lift. The vortex model is matched to the measured rotary balance data, and once a satisfactory match has been estimated, small disturbances in angular body rates are applied and associated changes in aerodynamic coefficients are calculated to provide disturbance moment derivatives in Equation 26. The disturbance moment coefficients are calculated over the full range of  $\alpha$  and  $\frac{\Omega b}{2V}$  to create the necessary data base. The effect of  $\beta$  is neglected. Before this data base can be accessed the aircraft rotary and disturbance rotation rates must be calculated. A report on this computational procedure is in preparation.

## 6 EXAMPLE APPLICATION OF THE SPIN MODEL

### 6.1 Equilibrium Spin Prediction

The flight dynamic spin model can be used to calculate possible spin modes through the use of the trimming routines explained in Section 4.1. Table 1 shows a comparison of a spin mode given in Reference 5, calculated by the same technique used by the present model for the initial trim, and the same spin mode calculated with the flight dynamic spin model. Other modes can be identified by changing the setting of the control deflections. Note the difference between the spin prediction of FDSM(1) and FDSM(2) of Table 1. The spin trim equations of Section 4.1 are represented by FDSM(1) and assume that all side forces are zero. FDSM(2) however, represents the full flight dynamic spin equations of motion and does include side force effects.

Table 1: Spin Prediction Comparison

	$\alpha$	$\frac{R_s}{V}$	$V$	$\beta$	$R_s$
Ref. 5	48	0.28	48	-4	1.4
FDSM(1)*	47.5	0.276	46.0	-3.58	1.48
FDSM(2)**	49.6	0.341	44.3	-5.14	1.00

(for  $\delta_e = -25^\circ$ ,  $\delta_r = -25^\circ$ ,  $\delta_a = 0^\circ$ )

\* Initial spin approximation

\*\* POWIT 6 d.o.f. trim

### 6.2 Spin Manoeuvre

To show the full capability of the flight dynamic spin model a manoeuvre that covers both rectilinear and spinning flight will be presented as an example. Figures 11 - 16 show the time history traces for the manoeuvre which is constructed as follows.

Firstly, the flight dynamic spin model is trimmed in rectilinear flight for a flight path velocity of 90 kts and at an altitude of 10000 ft. The trim results are  $\alpha = 8.2^\circ$ ,  $\gamma = -6.7^\circ$  with the powerplant thrust set to be zero, and the control trim values  $\delta_e = -2.6^\circ$ ,  $\delta_r = 1.8^\circ$ , and  $\delta_a = -1.9^\circ$ . Note the offset in  $\delta_r$  and  $\delta_a$  required to balance non-zero lateral and directional moments measured in the RB test to keep the aircraft in a wing level descent.

With the aircraft in steady descent for 5 seconds the elevator is moved to  $\delta_e = -25^\circ$  at time  $t = 5$  seconds. The aircraft pitches up and stalls at about  $t = 6$  seconds at which time full starboard rudder is applied ( $\delta_r = -25^\circ$ ) to yaw the aircraft quickly and promote a fast spin entry. The controls remain fixed until time  $t = 45$  seconds when full anti-spin rudder is used ( $\delta_r = 25^\circ$ ) to recover from the spin. After another 3 seconds the aircraft has recovered but still slowly rolls until at time  $t = 48.5$  seconds the aircraft begins to roll in the opposite direction. At this

instant the elevator and rudder controls are brought to the initial trim values. The aircraft then dives, builds up speed and lift, then rounds out to almost level flight with a heading  $45^\circ$  starboard from where it started and has lost almost 9000 ft altitude. All these control deflections are shown in Figure 11.

Figure 12 shows the aircraft decreasing from 90 to 75 kts during the spin entry, while  $\alpha$  converges to  $48^\circ$  (expected from Table 1) and  $\gamma$  approaches  $-90^\circ$  (vertical descent). The velocity trace also shows the sharp increase during the recovery (almost 225 kts) and then a decrease as lift increases in the pull-out. Note that during the recovery stage (time  $t > 48.5$  seconds) that the high spin  $\alpha$  has returned to standard flight values of about  $3^\circ$  to  $5^\circ$ .

The time history traces of  $\frac{\partial \phi}{\partial t}$ ,  $\phi$ ,  $\theta$ ,  $\psi$  are shown in Figure 13. During the spin the spin rate converges to  $\frac{\partial \phi}{\partial t} = 0.36$ , then returns to zero at recovery. The oscillatory motion displayed during spin entry and recovery is due to a lowly damped Dutch roll mode. A more detailed investigation into the aerodynamic data at low  $\alpha$  will be reported later. Figure 14 shows the body rotation rates and normal acceleration during the manoeuvre. The pitch rate trace illustrates the sharp pitching due to the elevator control deflections at time  $t = 5$  seconds for the spin entry and at time  $t = 48.5$  seconds during the recovery. The yaw rate trace displays the high continuous yaw rates that can only be achieved during a spin (about 2.1 rad/sec). The dashed lines in the angular rotation rate manoeuvre traces represent the angular velocity components relative to axes aligned with the flight path vector while the solid lines represent the total angular rates. The difference between these two curves therefore represents the disturbance component of angular rotation rate given by the equations in Section 5. The difference between these curves for steady pitch rate arises because the RB contribution is related to the sideslip at zero spin radius (Equation (24)) while the total pitch rate is related to sideslip and to the helix angle associated with the spin-radius (see approximate Equation (14)). Aircraft position is shown in Figure 15 against time while Figure 16 plots altitude and displacement east (Y) against displacement north (X).

The time history traces provide a large amount of detailed information but do not quickly illustrate the flight path and aircraft attitudes during the manoeuvre. A general application graphics routine has been developed to read data, (not necessarily time history), and plot it in three dimensions (3D). Basically the graphics program reads a time history then plots the flight path on to which an aircraft image is overlaid at constant time intervals with full directional orientation.

The previous manoeuvre has been graphically illustrated in this way and is shown in Figures 17 - 20. The full manoeuvre is plotted in Figure 17 with an aircraft displayed every 2.5 seconds. The time interval must differ from the spin period which in this case is 2.3 sec/turn, or else the same view of the aircraft would be seen repeatedly.

The 3D plot now makes it easier to visualise the attitudes of the aircraft from trim to stall, spin entry to spin, and from spin to recovery. Figure 18 displays a

more detailed view of the spin entry and shows how the aircraft pitches up into a stall then banks to starboard as the rudder is applied. Figure 19 shows the aircraft attitudes in the steady spin, while Figure 20 details the recovery stage. The black outlined aircraft images displayed in the 3D plots, mark the point at which the anti-spin rudder was applied so that an idea of spin recovery time can be estimated.

## 7 CONCLUSION

A flight dynamic model of aircraft spinning has been developed. It is capable of simulating aircraft behaviour from conventional flight through stall, spin entry, steady spin, and spin recovery. A data base storage technique has been used to provide the six force and moment coefficients required. The data base embodies rotary balance data measured for a basic training aircraft plus computed disturbance data from a line vortex model. Details of the outputs from the flight dynamic model have been provided to illustrate the capabilities of the program to simulate spin entry and recovery. Time history output has been displayed using standard time history manoeuvre traces and also using detailed three dimensional plots of aircraft flight path and attitudes.

Many aspects of the presented approach to modelling aircraft spin have not been included in this report. Further work is in hand on several of them and will be reported later. The main aspects are:

- a) Details of the line vortex model used to calculate the small disturbance data,
- b) Effects of the cross-terms in the small disturbance coefficient matrix,
- c) The specific cause of the predicted oscillatory behaviour at about spin frequency during spin entry and recovery,
- d) Validation of the modelling by reference to dynamic testing on a  $\frac{1}{18}$ th scale model conducted at the NASA LRC. Full scale data are not available because the Wamira project did not proceed to the flight prototype stage. Reference 12 discusses the model application to spin recovery.

## REFERENCES

1. GIBBENS, P.W. ; A Flight Dynamic Simulation Program in Air-path Axes using A.C.S.L. ARL-AERO-TM-380. June 1986.
2. Advanced Continuous Simulation Language (ACSL), Mitchell & Gauthier Associates, Inc
3. MARTIN, C.A. ; Modelling Aircraft Dynamics. ARL-AERO-TECH-MEMO-400 July 1988
4. HULTBERG, R.S. ; Rotary Balance Data and Analysis for the Australian Aircraft Consortium Mk-1 Trainer. BAR 83-7, August 1983.
5. MARTIN, C.A. and SECOMB, D.A. ; RAAF BPTA Phase II Wind Tunnel Tests: Rotary Balance Tests, May/June 1983 Part1. Unpublished data report.
6. MARTIN, C.A. and SECOMB, D.A. ; RAAF BPTA Phase II Wind Tunnel Tests: Rotary Balance Tests, May/June 1983 Part2 - Data Charts. Unpublished data report.
7. BIHRLE Jr, W. and BARNHART, B. ; Spin Prediction Techniques. Journal of Aircraft Volume 20, Number 2, February 1983, Page 97.
8. FLETCHER, C.A.J. ; POWITT - A Program for Solving Non-Linear Algebraic Equations. WRE-TN-1431 (WR&D), June 1975.
9. MAINE, R.E. and ILIFF, K.W. ; Identification of Dynamic Systems: Theory and Formulation. NASA Reference Publication 1138, February 1985.
10. SCHER, S. H. ; An Analytical Investigation of Airplane Spin-Recovery Motion by use of Rotary-Balance Aerodynamic Data. NACA TN-3188, June 1954.
11. ETKIN, B. ; Dynamics of Atmospheric Flight. John Wiley & Sons, Inc., New York, 1972.
12. MARTIN C. A. and HILL S. D. ; Prediction of Aircraft Spin Recovery. AIAA-89-3363 FMC, August 1989.

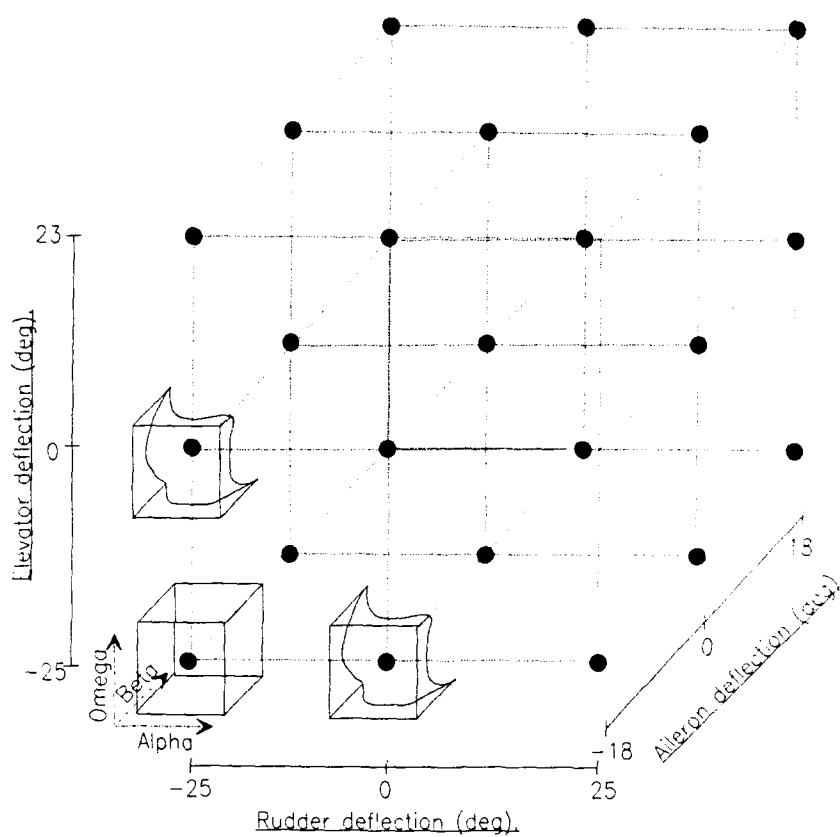


Figure 1. Data base schematic - phase 1.

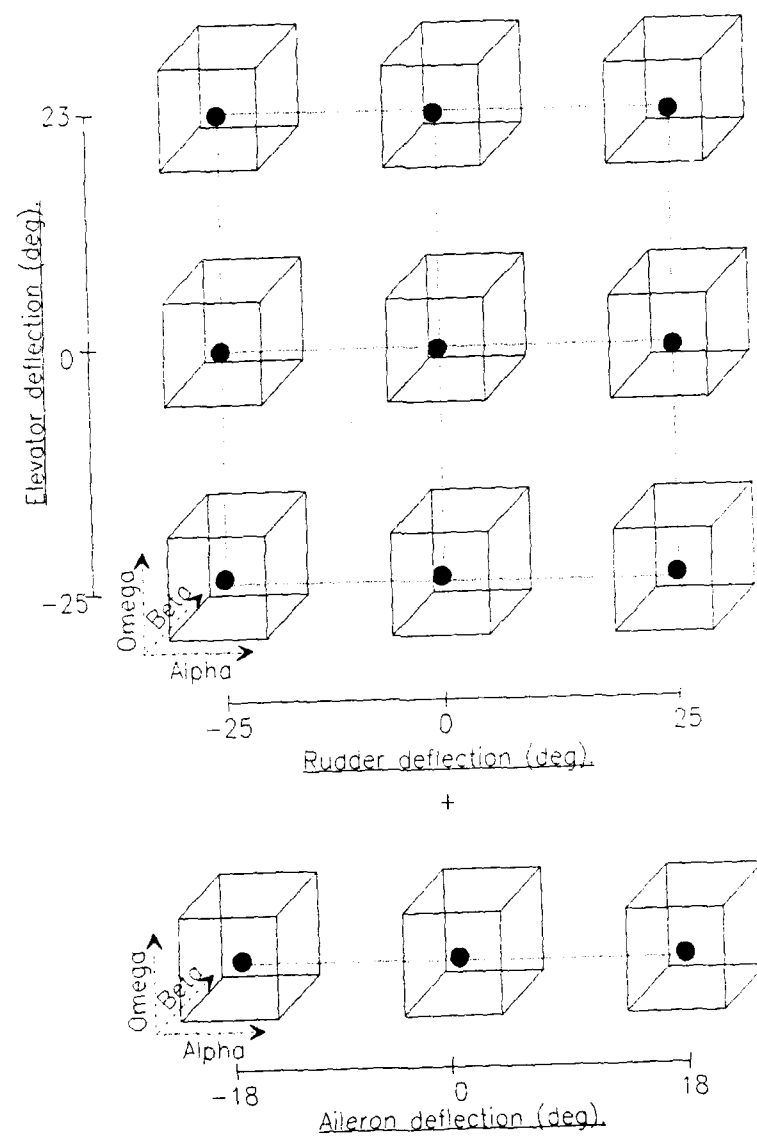


Figure 2. Data base schematic - phase 2.

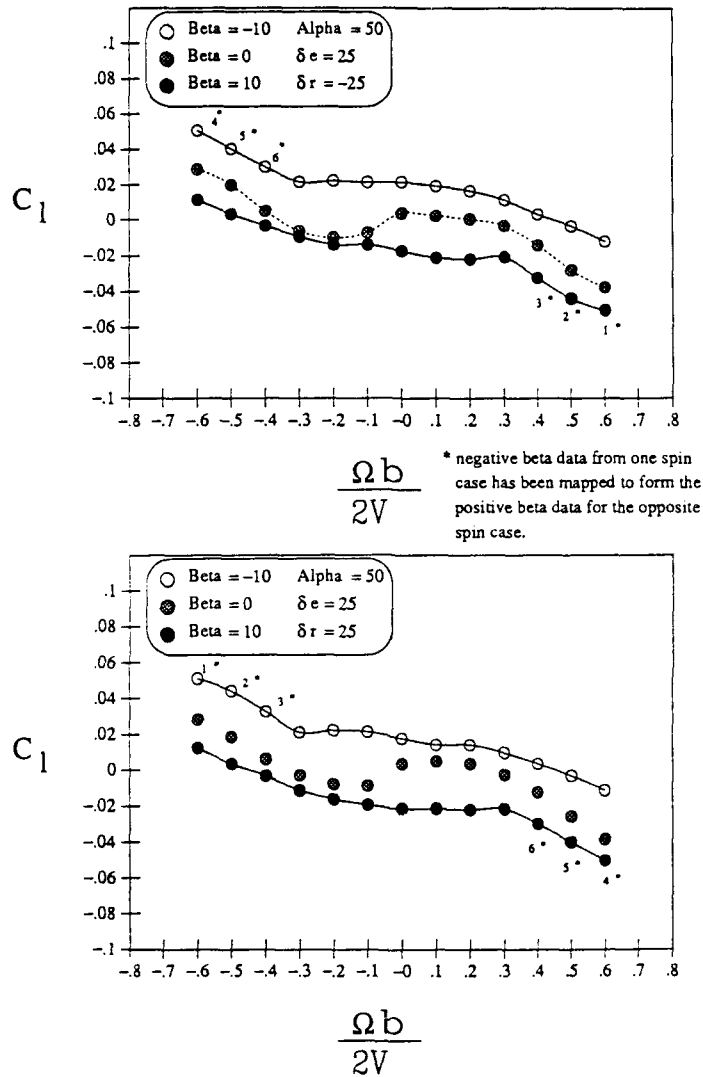


Figure 3. Method for creating positive sideslip data for rolling moment coefficient.

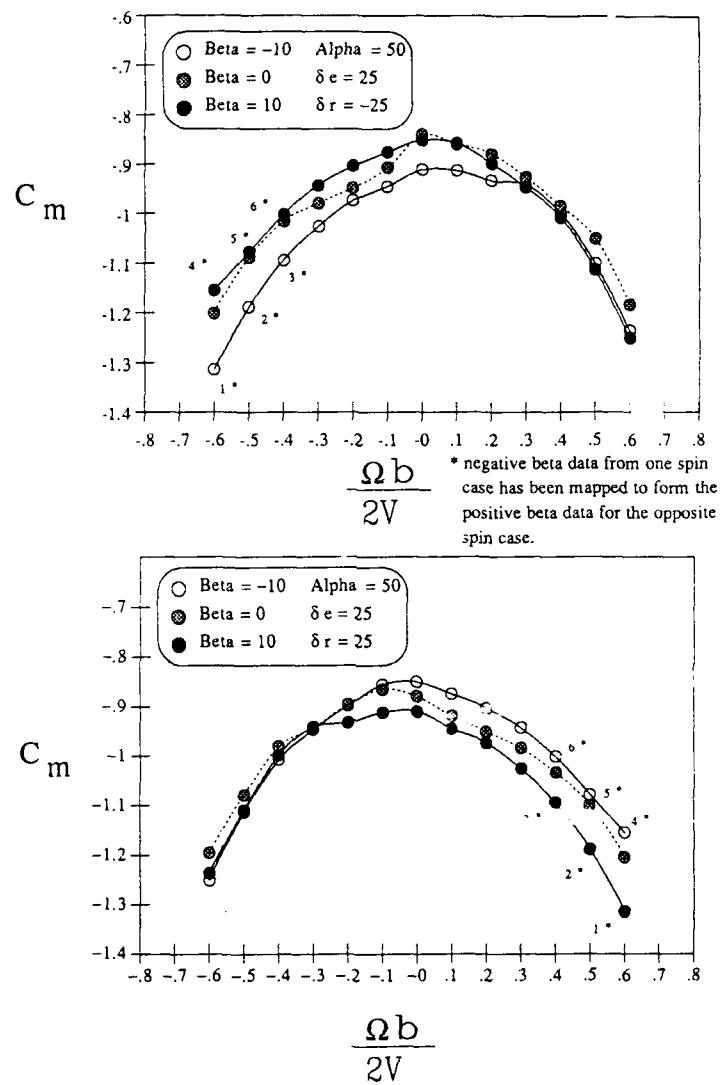


Figure 4. Method for creating positive sideslip data for pitching moment coefficient.

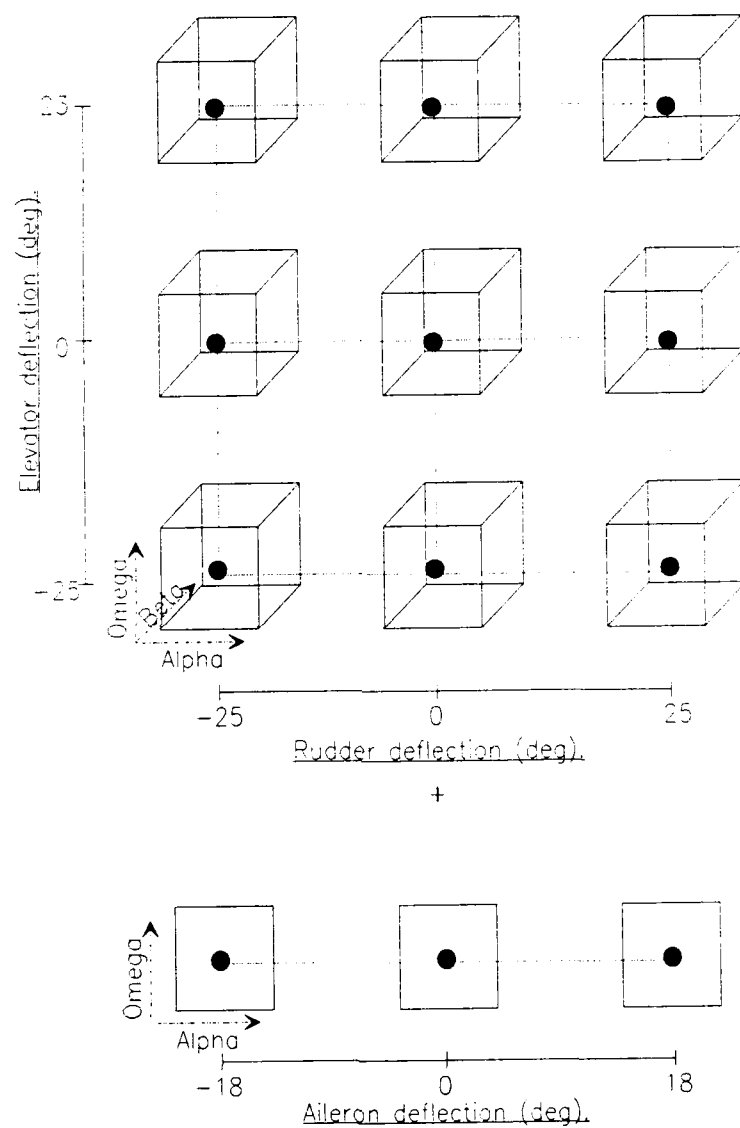


Figure 5. Data base schematic - phase 3

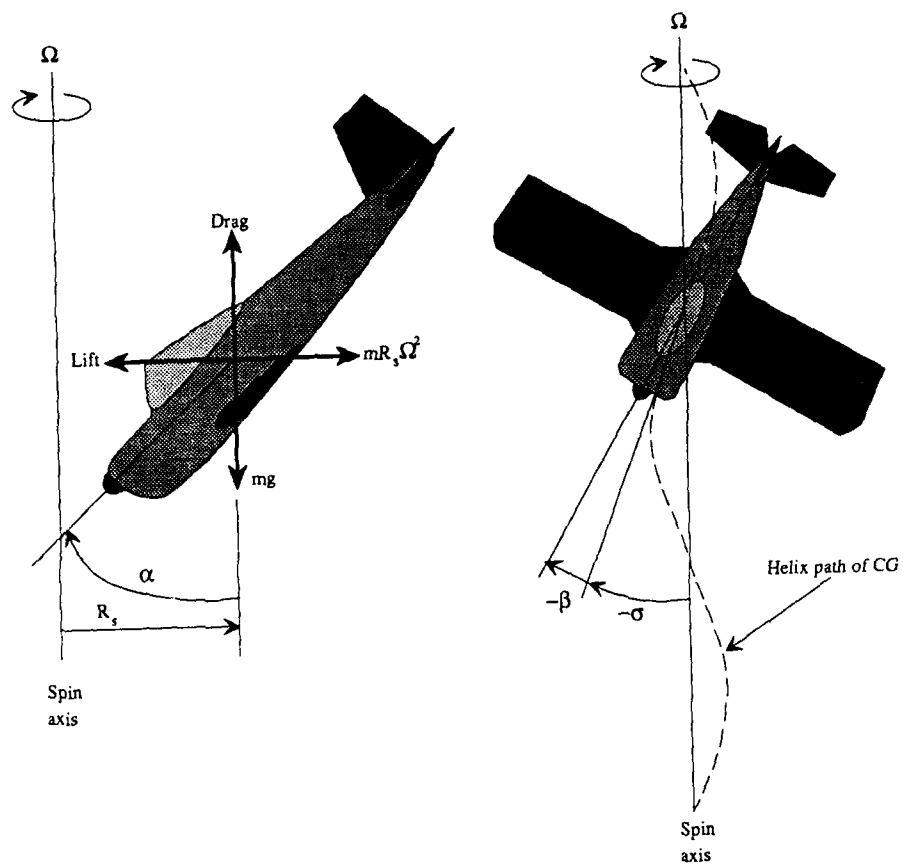


Figure 6. Illustration of aircraft in steady spin.

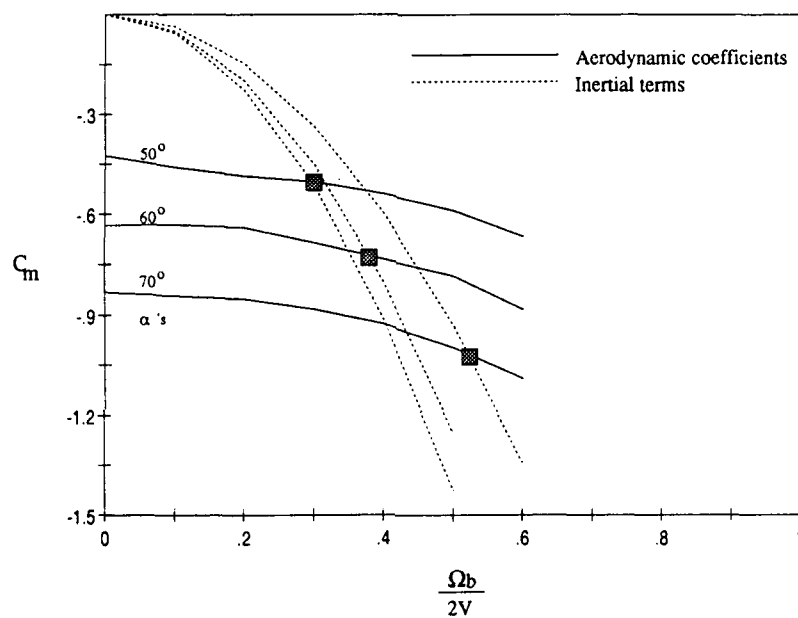


Figure 7. Pitching moment coefficient and inertial roll terms vs non-dimensional spin rate for selected angles of attack and zero sideslip.

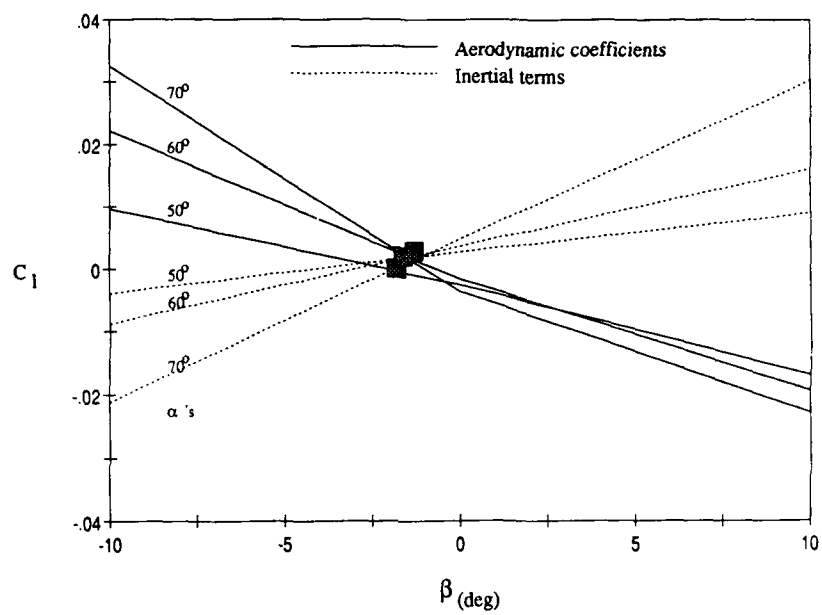


Figure 8. Rolling moment coefficient and inertial terms vs sideslip for selected angles of attack.

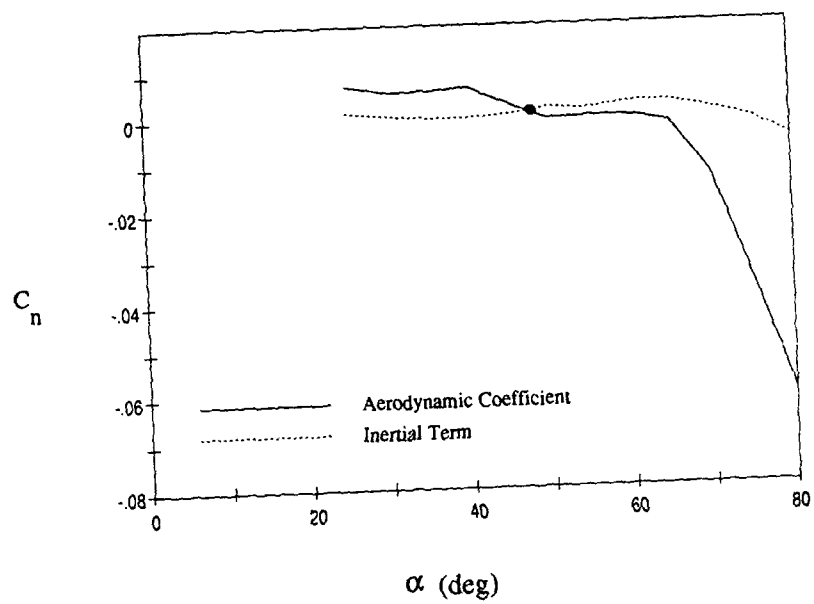


Figure 9. Yawing moment coefficient and inertial terms vs angle of attack identifying spin equilibrium angles of attack.

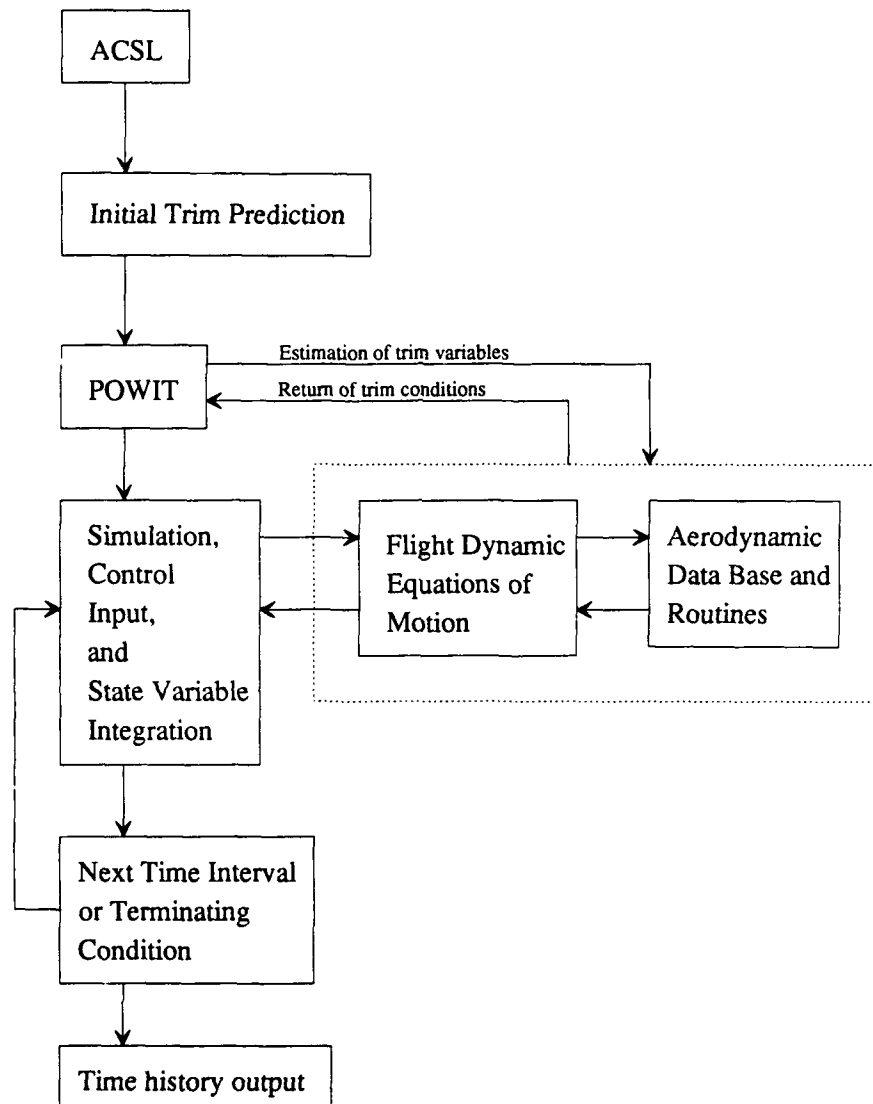


Figure 10. Flight dynamic spin model block diagram.

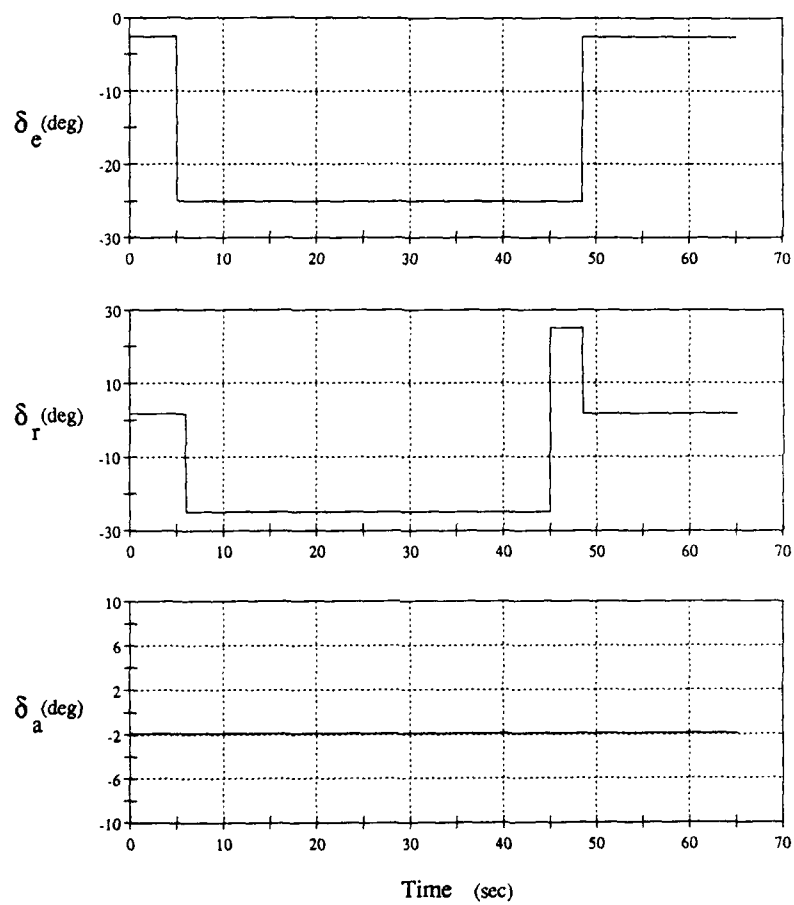


Figure 11. Manoeuvre control inputs for elevator, rudder, and aileron.

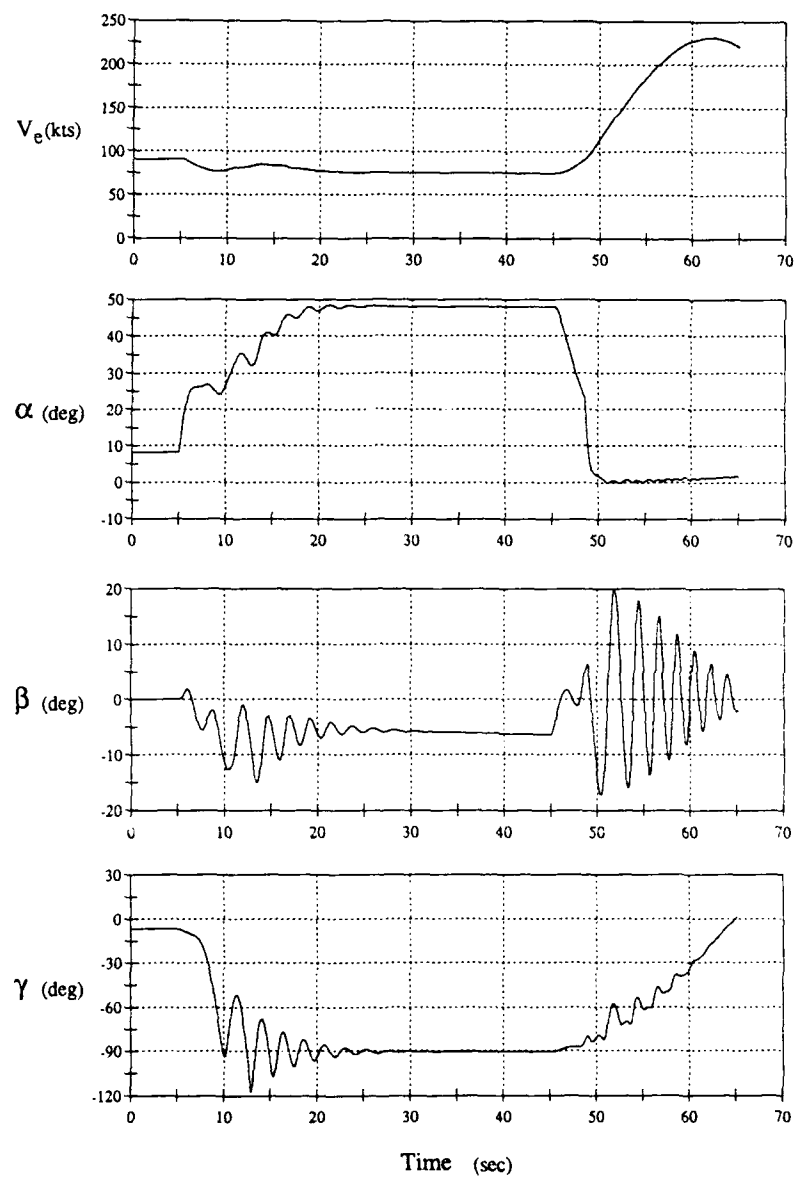


Figure 12. Manoeuvre time history traces.

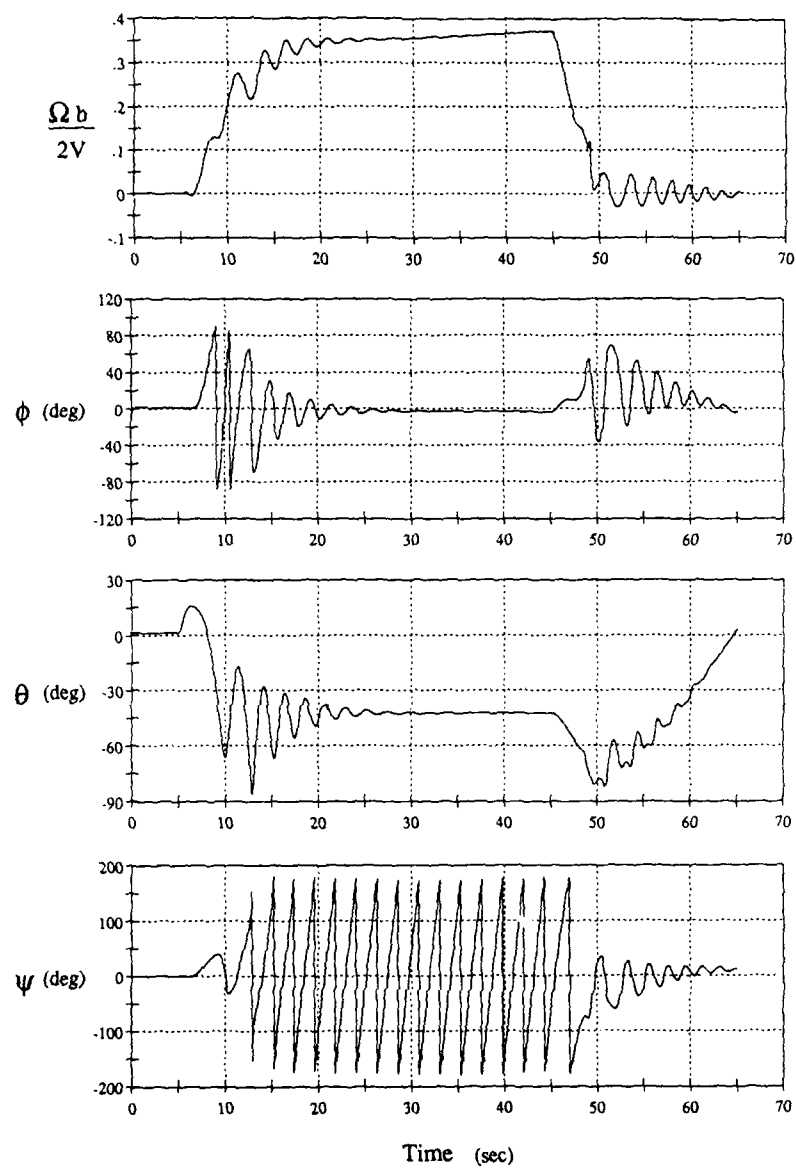


Figure 13. Manoeuvre time history traces.

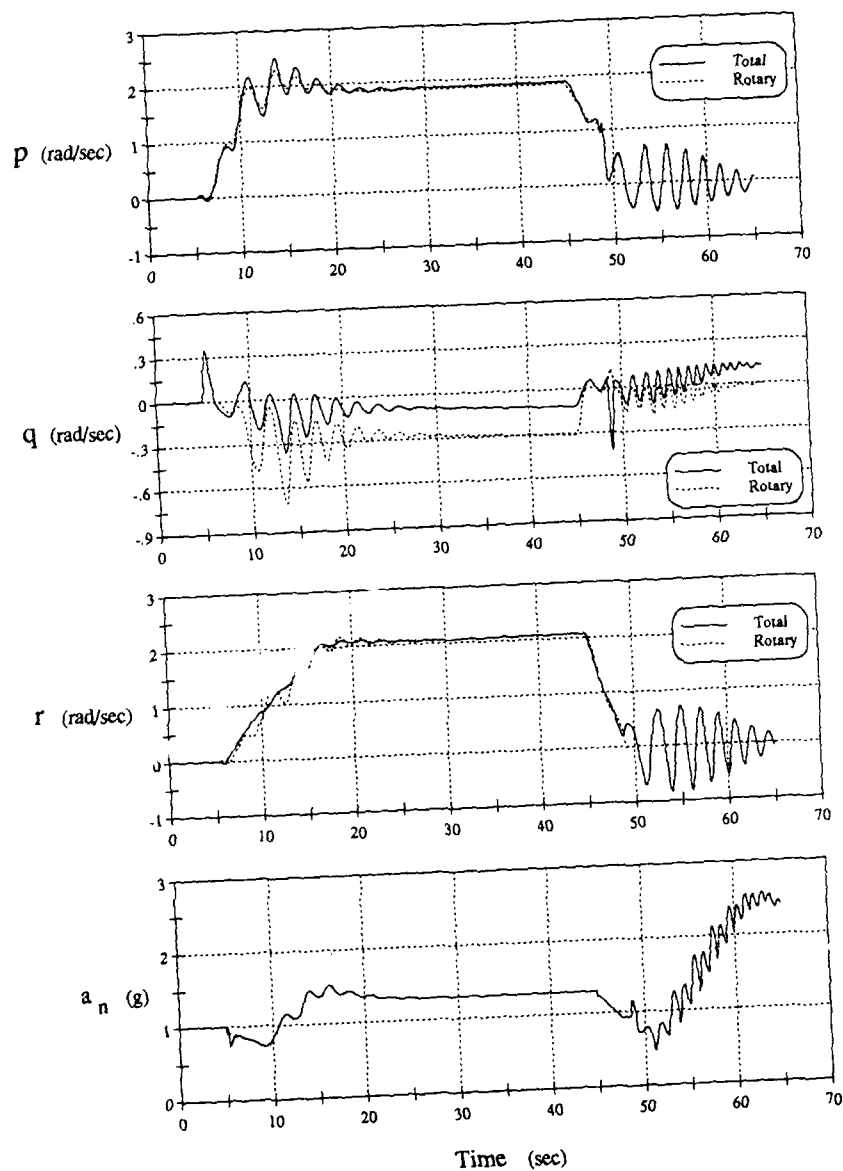


Figure 14. Manoeuvre time history traces.

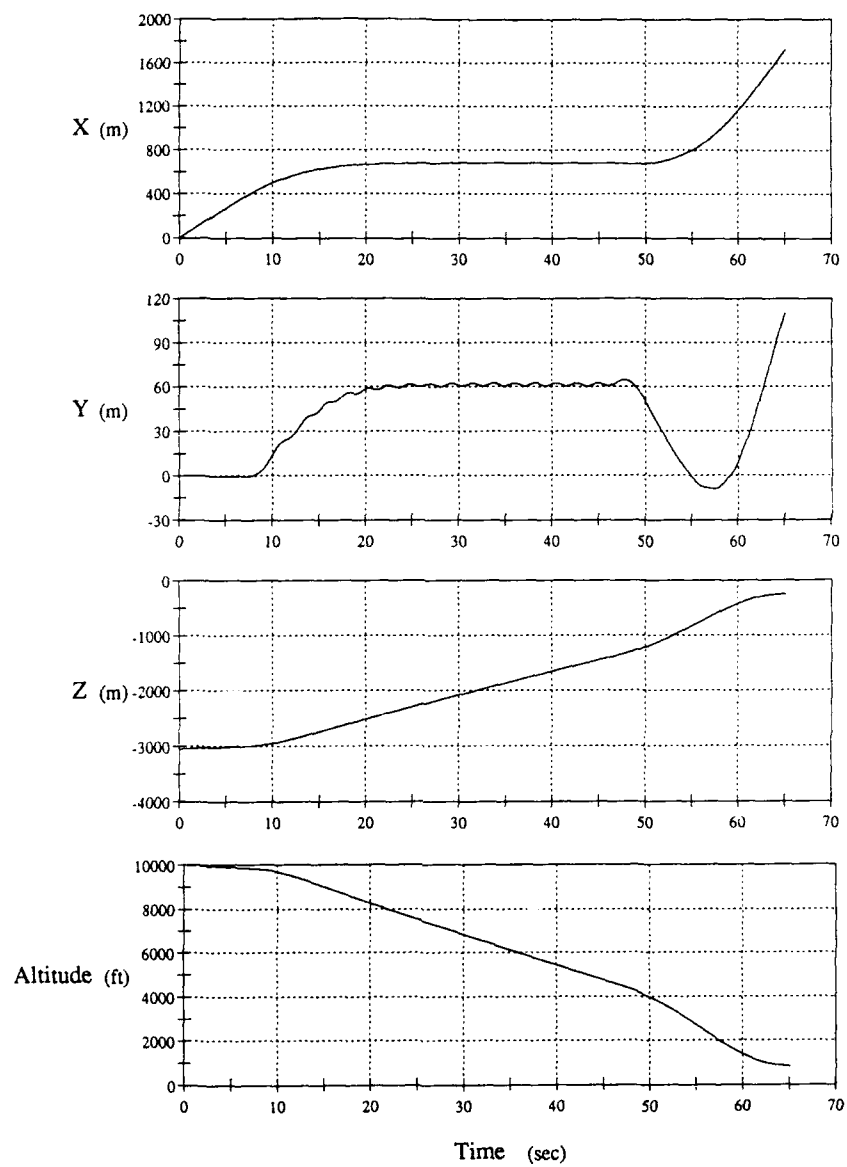


Figure 15. Manoeuvre time history traces.

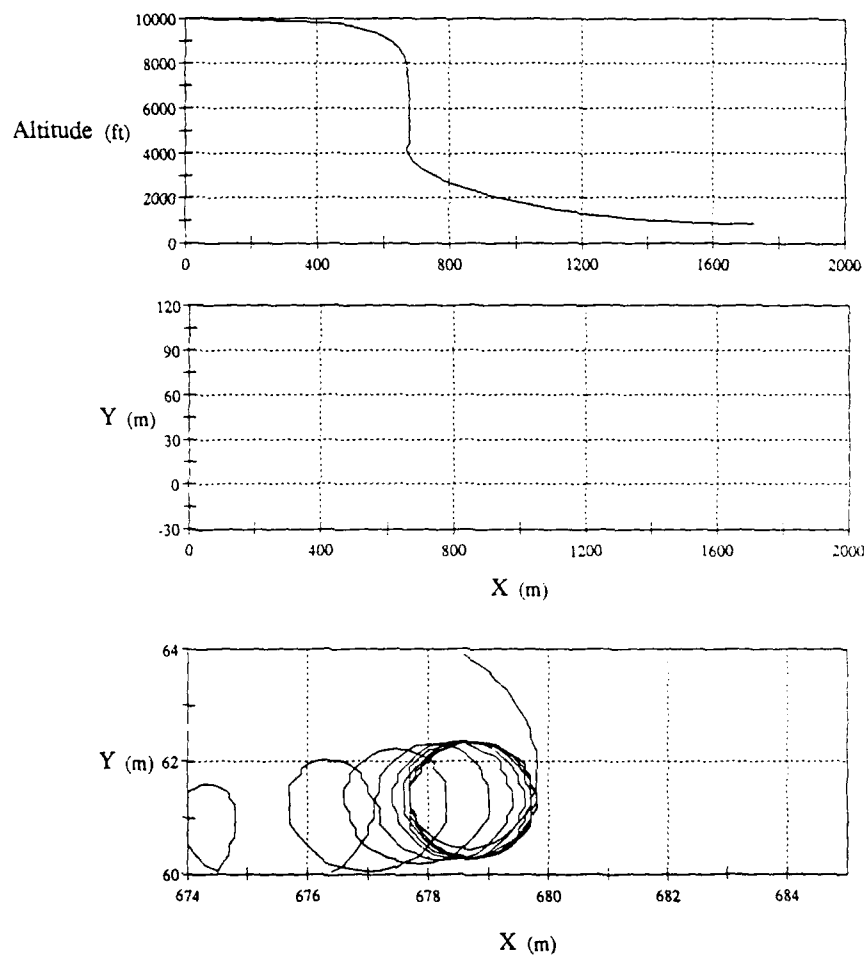


Figure 16. Manoeuvre trajectory.

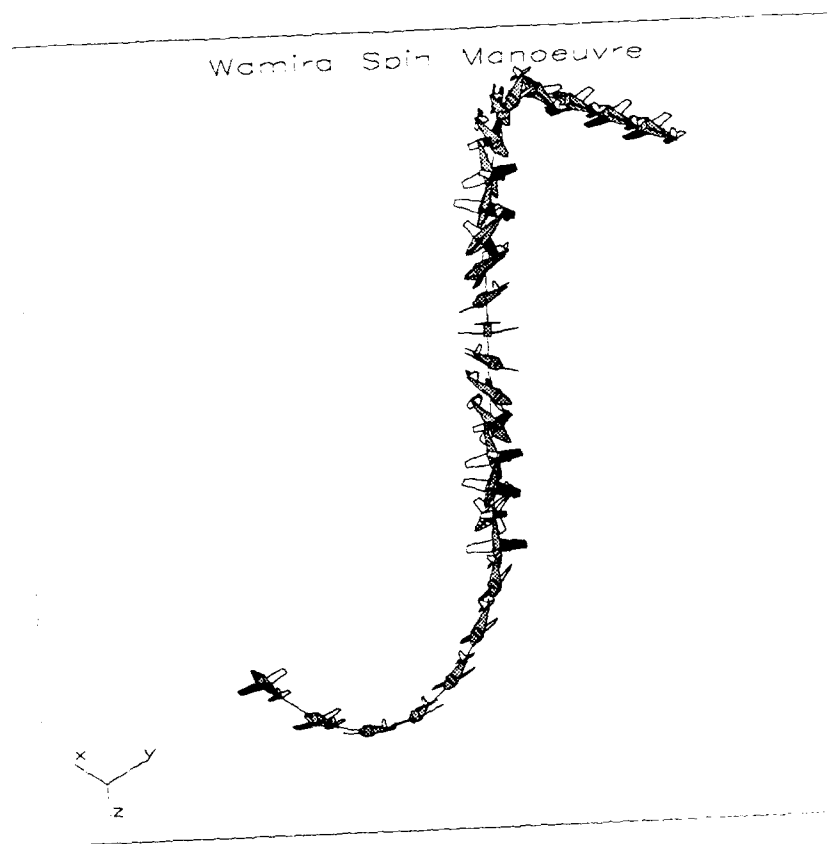


Figure 17. Three dimensional plot of aircraft manoeuvre.



Figure 18. Three dimensional plot of aircraft spin entry.

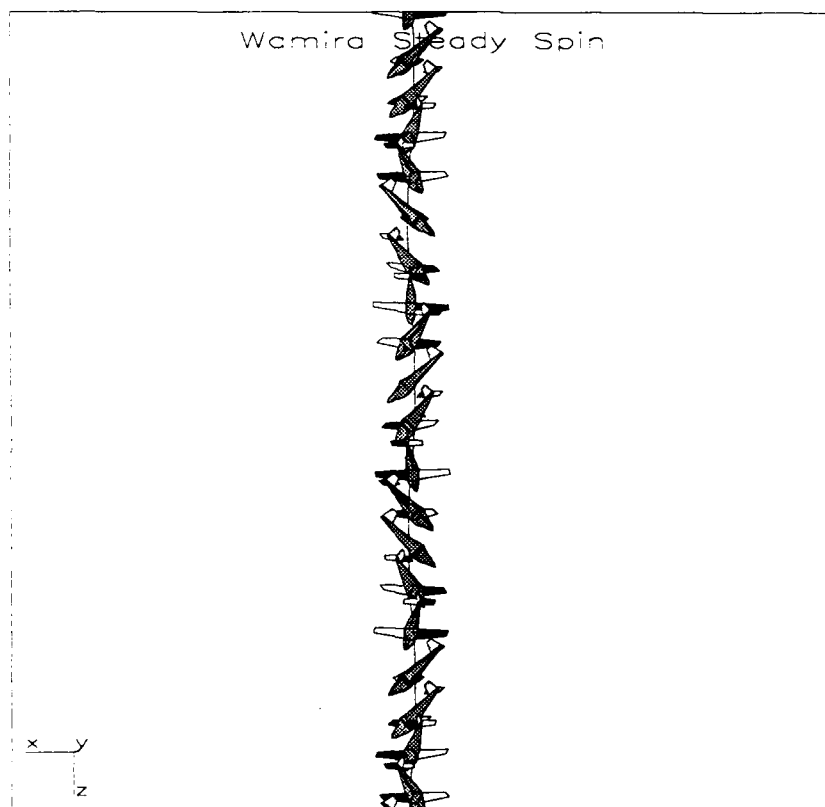


Figure 19. Three dimensional plot of aircraft steady spin.

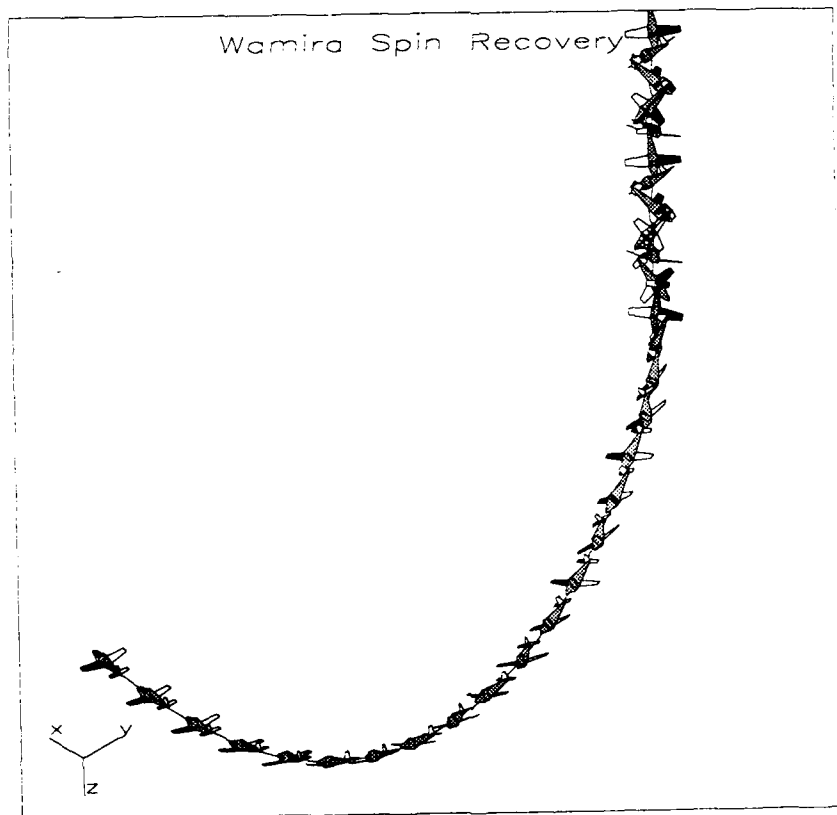


Figure 20. Three dimensional plot of aircraft recovery.

## DISTRIBUTION

### AUSTRALIA

#### DEPARTMENT OF DEFENCE

##### DEFENCE CENTRAL

Chief Defence Scientist  
AS, Science Corporate Management (shared copy)  
FAS, Science Policy (shared copy)  
Director, Departmental Publications  
Counsellor, Defence Science, London (Doc Data sheet only)  
Counsellor, Defence Science, Washington (Doc Data sheet only)  
SA to the Thailand Military R and D Centre (Doc Data sheet only)  
SA to the D R C (Kuala Lumpur) (Doc Data sheet only)  
OIC TRS, Defence Central Library  
Document Exchange Centre, DISB (18 copies)  
Joint Intelligence Organisation  
Librarian H Block, Victoria Barracks, Melbourne  
Director General - Army Development (NSO) ( 4 copies)  
Defence Industry and Materiel Policy, FAS

##### AERONAUTICAL RESEARCH LABORATORY

Director  
Library  
Chief - Flight Mechanics and Propulsion Division  
Head - Flight Mechanics Branch  
Branch File - Flight Mechanics  
Authors: S.D. Hill  
          C.A. Martin  
J.S. Drobik  
M.I. Cooper  
L.D. Maclaren  
M.I. Houston

##### MATERIALS RESEARCH LABORATORY

Director/Library

##### DEFENCE SCIENCE & TECHNOLOGY ORGANISATION - SALISBURY

Library

##### NAVY OFFICE

Navy Scientific Adviser (3 copies Doc Data sheet)  
Aircraft Maintenance and Flight Trials Unit  
Director Naval Engineering Requirements - Aviation Systems

##### ARMY OFFICE

Scientific Adviser - Army (Doc Data sheet only)

##### AIR FORCE OFFICE

Air Force Scientific Adviser (Doc Data sheet only)  
Aircraft Research and Development Unit  
Scientific Flight Group  
Library  
Engineering Branch Library  
Director General Engineering - Air Force  
HQ Logistics Command [SLENGO]

##### DEPARTMENT OF TRANSPORT & COMMUNICATION

Library

#### STATUTORY AND STATE AUTHORITIES AND INDUSTRY

Aerospace Technologies of Australia P/L - Manager/Library (2 copies)  
Ansett Airlines of Australia, Library  
Australian Airlines, Library  
Qantas Airways Limited  
Hawker de Havilland Aust. Pty Ltd, Victoria, Library  
Hawker de Havilland Aust. Pty Ltd, Bankstown, Library  
Rolls Royce of Australia Pty Ltd, Manager

#### UNIVERSITIES AND COLLEGES

Adelaide  
Barr Smith Library  
Professor of Mechanical Engineering

Flinders  
Library

La Trobe  
Library

Melbourne  
Engineering Library

Monash  
Hargrave Library  
Professor I J Polmear, Materials Engineering

Newcastle  
Library ( 2 copies)

New England  
Library

Sydney  
Engineering Library  
Head, School of Civil Engineering  
D. Auld, Aeronautical Engineering

NSW  
Physical Sciences Library  
Professor R A A Bryant, Mechanical Engineering  
Library, Australian Defence Force Academy

Queensland  
Library

Tasmania  
Engineering Library

Western Australia  
Library  
Professor B.J. Stone, Head Mechanical Engineering

RMIT  
Library  
Mr M. Scott, Aerospace Engineering

University College of the Northern Territory  
Library

CANADA

CAARC Coordinator Aerodynamics

National Aeronautical Establishment  
Head, Unsteady Aerodynamics Laboratory

NRC

Aeronautical & Mechanical Engineering Library

UNIVERSITIES AND COLLEGES

Toronto

Institute for Aerospace Studies

FRANCE

ONERA, Library

GERMANY

Fachinformationszentrum: Energie, Physic, Mathematik GMBH

INDIA

CAARC Coordinator Aerodynamics

National Aeronautical Laboratory, Information Centre

ISRAEL

Technion-Israel Institute of Technology  
Professor J Singer

ITALY

Professor Ing. Guiseppe Gabrielli

JAPAN

National Aerospace Laboratory

UNIVERSITIES

Kagawa University  
Professor H Ishikawa

NETHERLANDS

National Aerospace Laboratory [NLR], Library

NEW ZEALAND

Defence Scientific Establishment, Library  
RNZAF, Vice Consul (Defence Liaison)

UNIVERSITIES

Canterbury  
Library  
Professor D Stevenson, Mechanical Engineering

SWEDEN

Aeronautical Research Institute, Library  
Swedish National Defense Research Institute (FOA)

SWITZERLAND

F + W (Swiss Federal Aircraft Factory)

#### UNITED KINGDOM

CAARC Coordinator Aerodynamics  
Royal Aircraft Establishment  
Bedford, Library  
Pyestock, Director  
Farnborough, Aerodynamics Department  
Dr A.J. Ross  
National Physical Laboratory, Library  
British Library, Document Supply Centre  
Aircraft Research Association, Library  
British Aerospace  
Kingston-upon-Thames, Library  
Hatfield-Chester Division, Library  
Short Brothers Ltd, Technical Library

#### UNIVERSITIES AND COLLEGES

Bristol  
Engineering Library

Cambridge  
Library, Engineering Department  
Whittle Library

London  
Professor G J Hancock, Aero Engineering

Manchester  
Professor D. I. A. Poll, Dept of Engineering (Aeronautical)

Southampton  
Library

Liverpool  
Fluid Mechanics Division, Dr J C Gibbings

Strathclyde  
Library

Cranfield Inst. of Technology  
Library

Imperial College  
Aeronautics Library

#### UNITED STATES OF AMERICA

AFWAL/FIMM, Mr R.F. Osborne  
NASA Scientific and Technical Information Facility  
NASA Langley  
Mr J.R. Chambers  
Mr J.S. Bowman  
Mr L.T. Nguyen  
Professor V. K. Klein  
NASA Ames, Dr L.B. Schiff  
Boeing Company  
Dr M. R. Johnson - Director Structures Engineering  
Lockheed-California Company  
McDonnell Aircraft Company, Library  
David Taylor Naval Ship R&D Center, Mr J.H. Nichols

## UNIVERSITIES AND COLLEGES

Chicago  
John Crerar Library

Florida  
Aero Engineering Department  
Professor D C Drucker

Iowa State  
Dr G K Serovy, Mechanical Engineering

Iowa  
Professor R I Stephens

Princeton  
Professor R.F. Stengle, Mechanical and Aerospace Engineering

Maryland  
Professor J. Barlow, Aerospace Engineering

Massachusetts Inst. of Tech.  
MIT Libraries

Spares ( 10 copies)

Total (150 copies)

**DOCUMENT CONTROL DATA**PAGE CLASSIFICATION  
**UNCLASSIFIED**

PRIVACY MARKING

1a. AR NUMBER <b>AR-005-600</b>	1b. ESTABLISHMENT NUMBER <b>ARL-FLIGHT-MECH-R-180</b>	2. DOCUMENT DATE <b>JUNE 1990</b>	3. TASK NUMBER <b>DST 89/074</b>
4. TITLE <b>A FLIGHT DYNAMIC MODEL OF AIRCRAFT SPINNING</b>		5. SECURITY CLASSIFICATION (PLACE APPROPRIATE CLASSIFICATION IN BOX(S) IE. SECRET (S), CONF (C), RESTRICTED (R), UNCLASSIFIED (U)).  <div style="display: flex; justify-content: space-around;"> <div style="border: 1px solid black; padding: 2px; text-align: center;">U</div> <div style="border: 1px solid black; padding: 2px; text-align: center;">U</div> <div style="border: 1px solid black; padding: 2px; text-align: center;">U</div> </div> DOCUMENT      TITLE      ABSTRACT	6. NO. PAGES  <b>39</b>  7. NO. REFS  <b>12</b>
8. AUTHOR(S) <b>S.D. Hill C.A. Martin</b>		9. DOWNGRADING/DELIMITING INSTRUCTIONS  <b>Not applicable</b>	
10. CORPORATE AUTHOR AND ADDRESS <b>AERONAUTICAL RESEARCH LABORATORY P.O. BOX 4331, MELBOURNE VIC 3001</b>		11. OFFICE/POSITION RESPONSIBLE FOR SPONSOR <b>DSTO</b>  SECURITY _____  DOWNGRADING _____  APPROVAL <b>DARL</b>	
12. SECONDARY DISTRIBUTION (OF THIS DOCUMENT) <b>Approved for public release.</b>  OVERSEAS ENQUIRIES OUTSIDE STATED LIMITATIONS SHOULD BE REFERRED THROUGH DSTIC, ADMINISTRATIVE SERVICES BRANCH II, DEPARTMENT OF DEFENCE, ANZAC PARK WEST OFFICES, ACT 2601			
13a. THIS DOCUMENT MAY BE ANNOUNCED IN CATALOGUES AND AWARENESS SERVICES AVAILABLE TO:  <b>No limitations</b>			
13b. CITATION FOR OTHER PURPOSES (IE. CASUAL ANNOUNCEMENT) MAY BE <input checked="" type="checkbox"/> UNRESTRICTED OR <input type="checkbox"/> AS FOR 13a			
14. DESCRIPTORS <b>Aircraft spin Flight dynamics Model theory</b>			15. DISCAT SUBJECT CATEGORIES  <b>0101</b>
16. ABSTRACT <b>A flight dynamic model of aircraft spinning been developed. It is capable of simulating aircraft behaviour from conventional flight through stall, spin entry, steady spin, and spin recovery. A data base storage technique has been used to provide the six force and moment coefficients required. The data base embodies rotary balance data measured for a basic training aircraft plus computed small disturbance data calculated from a line vortex model.</b>			

PAGE CLASSIFICATION  
UNCLASSIFIED

PRIVACY MARKING

THIS PAGE IS TO BE USED TO RECORD INFORMATION WHICH IS REQUIRED BY THE ESTABLISHMENT FOR ITS OWN USE BUT WHICH WILL NOT BE ADDED TO THE DISTIS DATA UNLESS SPECIFICALLY REQUESTED.

16. ABSTRACT (CONT).

17. IMPRINT

**AERONAUTICAL RESEARCH LABORATORY, MELBOURNE**

18. DOCUMENT SERIES AND NUMBER

FL : Mechanics Report 180

19. COST CODE

52 5235

20. TYPE OF REPORT AND PERIOD COVERED

21. COMPUTER PROGRAMS USED

22. ESTABLISHMENT FILE REF.(S)

23. ADDITIONAL INFORMATION (AS REQUIRED)